Topology optimized design, microfabrication and characterization of electro-thermally driven microgripper

Rubio, Wilfred M.; Silva, Emilio C.N.; Bordatchev, Evgueni V.; Zeman, Marco

Publisher's version / Version de l'éditeur:
https://doi.org/10.1177/1045389X08093548
Journal of Intelligent Material Systems and Structures, 20, 6, 2008-09-22

Topology Optimized Design, Microfabrication and Characterization of Electro-Thermally Driven Microgripper

WILFREDO M. RUBIO*, EMILIO C. N. SILVA
Department of Mechatronics and Mechanical Systems Engineering
Escola Politécnica da Universidade de São Paulo
Av. Prof. Mello Moraes, 2231 - Cidade Universitária, São Paulo – SP – 05508-900, Brazil
wilfredo.rubio@poli.usp.br, ecnsilva@usp.br

EVGUENI V. BORDATCHEV, MARCO ZEMAN
Integrated Manufacturing Technologies Institute
National Research Council of Canada
800 Collip Circle, London, Ont., Canada
{evgueni.bordatchev, marco.zeman}@nrc.gc.ca

March 2007

Submitted to: Journal of Intelligent Material Systems and Structures

For correspondence:
Wilfredo M. Rubio

Tel: 55-11-30915419
Fax: 55-11-30915461
E-mail: wilfredo.rubio@poli.usp.br

* corresponding author, e-mail: wilfredo.rubio@poli.usp.br, phone: 55-11-30915419

Abstract

Micro-mechanical operations, e.g. actuating, rotational, tilting, and tweezing motions, produced by microactuators, microgrippers and microtweezers are essentially required for micro- handling, manipulation and assembly of miniature mechanical parts, biological samples, living cell, bacteria, tissues, *etc.* This paper presents a systematic and logical study of the topology optimized design, microfabrication, and static/dynamic performance characterization of an electro-thermo-mechanical microgripper. The microgripper is designed using a continuum topology optimization algorithm based on a spatial filtering technique and considering different penalization coefficients for different material properties during the optimization cycle. The microgripper design has a symmetric monolithic 2-D structure as a complex combination of rigid links integrating both the actuation and gripping mechanisms. The numerical simulation is performed by studying the effects of convective heat transfer, thermal boundary conditions at the fixed anchors, and microgripper performance considering temperature-dependent and independent material properties. The microgripper is fabricated from a 25 μm thick nickel foil using laser microfabrication technology and its static/dynamic performance is experimentally evaluated. The static and dynamic electro-mechanical characteristics are analyzed as step responses functions with respect to tweezing/actuating displacements, applied current/power, and actual electric resistance. A microgripper prototype having overall dimensions of 1 mm (L) x 2.5 mm (W) is able to deliver the maximum tweezing and actuating displacements of 25.5 μm and 33.2 μm along X and Y axes, respectively, under an applied power of 2.32 W. Experimental performance is compared with finite element modeling simulation results.

Keywords:
micro-electro-mechanical systems, microgripper, topology optimization, laser microfabrication, performance characterization, finite element modelling

1 Introduction

Electro-thermally driven micro-mechanisms, such as microactuators and microgrippers, are typical representatives of functional micro-electro-mechanical systems (MEMS) that function based on electro-thermo-mechanical transformation generated by the Joule heating effect producing required mechanical operations, e.g. linear, rotary, tilting or tweezing motions. These microsystems are in demand for micro- handling, manipulation and assembly of miniature mechanical parts, biological samples, living cell, bacteria, tissues, *etc.*, e.g. blood vessel manipulation (Wierzbicki, *et al.*, 2006), assembly of miniaturized endoscopic devices (Menciassi, *et al.*, 2004).

Typically, a microgripper is composed of an actuating mechanism (actuator) as a source of motions, which are transformed into gripping/releasing motions by a gripping mechanism with gripping pads. In a case of advanced gripping system, a sensor for measuring actual gripping force and displacements is integrated into one solid structure (Park and Moon, 2003). Several microfabrication techniques are usually employed to manufacture microgrippers, mainly, laser micromachining technology (Bordatchev *et al.*, 2004), LIGA procedure, electro-discharge-machining (Goldfarb and Celanovic, 1999) and IC-based silicon processing (Roch *et al.*, 2003).

The mechanical and non-mechanical methods are generally used for gripping functions of the end-effectors. The mechanical gripping is based on mechanical force contact between a micro-object and gripping pads, e.g., grasping by a needle tip (Menciassi *et al.*, 2004), by one or three tweezing fingers (Menciassi *et al.*, 2004; Park and Moon, 2005); and mostly used by a pair of tweezing jaws (Bordatchev and Nikumb, 2005; Zeman *et al.*, 2006; Tsai *et al.*, 2005; Choi *et al.*, 2005; Nguyen *et al.*, 2004). The non-mechanical methods use different type of physical forces, such as, vacuum pressure force (Zesch *et al.*, 1997), magnetic force (Sanchez-Salmeron *et al.*, 2005) and surface tension force (Lambert *et al.*, 2006) to hold the micro-object.

There are more than ten types of actuation principles to drive microgrippers, but only five of them are commonly used in practical applications, they are – 1) electrostatic forces (Lee *et al.*, 2002, Volland *et al.*, 2002, Millet *et al.*, 2004), 2) piezoelectric deformations (Perez *et al.*, 2005; Goldfarb and Celanovic, 1999), 3) shape memory effect (Roch *et al.*, 2003), 4) electro-magnetic forces in Lorentz force-type actuators, e.g.., voice-coil motors (Kim *et al.*, 2004), and 5) electro-thermo-mechanical (ETM) deformations (Zeman *et al.*, 2006; Choi *et al.*, 2005; Bordatchev and Nikumb, 2005; Nguyen *et al.*, 2004). Each actuation principle has advantages and disadvantages and therefore should be properly chosen for particular application. Typical electrostatic actuators require very high voltages (50-100 V) which are not compatible with modern CMOS circuitry and provide relatively small output displacements. For example, the electrostatic gripper developed by Lee *et al.* (Lee *et al.*, 2002) requires 250 V generating an electric field across two electrostatic electrodes to grab a glass bead with a diameter of 170 μm, where a third electrode was actuated electro-thermally using 100 mA to push and release the glass bead. To improve the dynamic performance of the electrostatic actuators/grippers, a comb-type drive was used (Volland *et al*, 2002) still requiring high voltage in a range of 80 V providing displacements of up to 20 μm. Similarly, piezoelectric actuators require high voltages although offering high actuation forces, but they are not easy to fabricate and to integrate using conventional IC-based silicon microfabrication technologies. The ETM and shape-

memory alloys based microgrippers are more robust in terms of delivering large displacements but with lower actuation forces compared to piezoelectric actuators. Kohl *et al.* (Kohl *et al.,* 2000) developed a microgripper based on one-way shape memory effect and therefore required two separate actuation mechanisms for closing and opening of the gripping pads. A maximum stroke of 300 μm with an applied power of 80 mW was achieved. It is a general concern from users that ETM actuators and grippers require high operational temperatures. However, it is necessary to note that the microgripper's actuation component can operate with a maximum operational temperature of 59 °C (Kohl *et al.,* 2000). It should also be noted that the tweezing pads and ETM actuator are spatially separated, e.g. the closest distance between tweezing pads and actuator is at least 1 mm apart minimizing the effect of the heat generated by the ETM actuator.

The design of microgrippers itself is a separate area of the science of microsystems and it is not well developed yet. A literature review shows few attempts to systemize and generalize the principles of microgripper design. Generally, the science of microgripping systems is focused on analytical and/or finite element modelling, fabrication, grip-release methods, control, and materials studies, and therefore, the microgripper design is usually based on simple structural kinematics and intuitive approaches. However, due to the fact that microgripper performance involves complex multi-physics, mechanics, and dynamics, advanced design methodologies and systematic approaches should be used. Some of these methodologies are under development. Tsai *et al* (2005) systemized 28 planar compliant mechanisms suitable for two-finger microgrippers and proposed the transformation methodology for generating a wide variety of novel compliant microgripping mechanisms with prismatic input links. Choi *et al* (2005) developed a design algorithm based on the perturbation method using system identification parameters and model correlation. Another systematic and powerful tool, Topology Optimization Method (TOM), is used to determine solutions for complex multi-physics problems while designing electro-thermally driven microgrippers and other MEMS devices (Sigmund, 2001; Ananthasuresh, 2003). The TOM combines optimization algorithms with Finite Element Method (FEM).

This paper presents a complete cycle of an ETM microgripper development starting with optimal design using TOM and including finite element modelling, numerical simulations, high-precision microfabrication using laser micromachining technology, and comprehensive experimental performance evaluation. The microgripper design is developed using a continuum topology optimization algorithm based on a spatial filtering technique and considering different penalization coefficients for different material properties during the optimization cycle. The numerical simulations are performed by studying the effects of convective heat transfer, thermal boundary conditions at the anchors, and microgripper behavior with and without considering temperature-dependent material properties. In addition, the static and dynamic performances of the fabricated microgripper are studied and compared with the simulation results. This paper is organized as follows. Section 2 describes the topology optimization formulation for ETM microgripper and its design. Section 3 shows numerical simulation results of the topology optimized microgripper. The microfabrication details are presented in Section 4 followed by a comparison of the experimental and numerical results in Section 5. Finally, summary and conclusions are grouped in Section 6.

2 Topology Optimized Design of the ETM microgripper

2.1 Theoretical background

Topology Optimization Method is a powerful structural optimization technique that combines, in its conventional implementation, FEM with an optimization algorithm to find the optimal material distribution inside a given domain bounded by supports and applied loads, which must contain the unknown structure. One of the main concepts of the topology optimization is the *extended design domain* which is a large fixed geometric domain that must contain the whole structure to be determined by the optimization procedure including supports and loads applied. This concept of the topology optimization problem with respect to an ETM microgripper design is shown in Figure 1. The objective in the topological design problem is to determine the empty spaces and links of the structure by adding and removing material in this fixed geometric domain. Because the extended geometric domain is fixed, the finite element model is not changed during the optimization process that simplifies the calculation of derivatives of a continuous differentiable function defined over the extended domain.

['Insert Figure 1 about here']

Other topological optimization concept is based on the relaxation of the design domain or *material model*. The discrete problem (change of material from solid (one) to void (zero)), where the amount of material in each element can assume only values equal to either one or zero, is an ill-posed problem. A solution can be obtained by softening the problem with an assumption that the material has intermediate property values during the optimization process. This can be achieved by defining a material model with intermediate property values between 0 and 1 (Bendsøe and Sigmund, 2003).

In case of electro-thermally actuated microgripper design, TOM searches for a structural topology that maximizes a desired displacement, u_{out}, generated under an applied input voltage, V (see Figure 1). This optimization design problem is based on following FE formulation (Ananthasuresh, 2003):

$$K_0(\rho)U_0(\rho) = P_0 \quad \Rightarrow \quad \textbf{Electrical Analysis} \qquad (1)$$

$$K_1(\rho)U_1(\rho) = P_1(U_0(\rho), \rho) \quad \Rightarrow \quad \textbf{Thermal Analysis} \qquad (2)$$

$$K_2(\rho)U_2(\rho) = P_2(U_1(\rho), \rho) \quad \Rightarrow \quad \textbf{Elastic Analysis} \qquad (3)$$

where K_o and K_1 are the global electrical and thermal conductivity matrices, respectively; K_2 is the global stiffness matrix; U_o, U_1 and U_2 are the voltage, temperature and displacements output vectors, respectively, and, P_o, P_1 and P_2 are the electrical, thermal and structural load vectors, respectively. Note that the thermal analysis depends on the output voltage of the electrical problem, and the elastic analysis depends on output temperature of thermal problem. Since, in this implementation, the FE problem does not consider any coupling among electrical, thermal and elastic analysis, no variation of

the material properties with temperature is assumed, and no simultaneous solving of these equations is necessary. However, once the microgripper topology is obtained, several numerical simulations with realistic temperature-dependent material properties are necessary in order to evaluate the robustness and performance of a microgripper.

On the other hand, all the equilibrium equations are interdependent through the element relative density vector ρ, accordingly to the *material model*. In this work, the material properties are obtained from a material model based on Simple Isotropic Material Penalization (SIMP) (Bendsøe and Sigmund, 2003), which consists of three mathematical equations that state at each point of the domain (or each finite element) the local effective material properties are (Rubio, 2005):

$$\sigma_e(\rho^i) = (\rho^i)^{p_e}\sigma_e; \quad \sigma_t(\rho^i) = (\rho^i)^{p_t}\sigma_t; \quad E(\rho^i) = (\rho^i)^{p_m}E \tag{4}$$

where, σ_e, σ_t and E are the electrical and thermal conductivity, and Young's modulus of solid material (or without material model), respectively. The convection coefficient, γ, is assumed to be independent from the element density; otherwise, low-density elements would not be cooled (Sigmund, 2001). After the discretization, ρ^i is the design variable of the i-th finite element, called pseudo-density; thus, ρ^i describes the amount of material in each finite element having property values between 0 and 1. For ρ^i equal to 0, the material is equal to void, and for ρ^i equal to 1, the material is equal to solid material. p_e, p_t, p_m are the different penalization coefficients for "tuning" the intermediate property values during the optimization process.

2.2 Topology Optimization problem

The topology optimization problem for the ETM microgripper has the following specific requirements (see Figure 1):

- Gripping requirements: The object should be grasped at the desired position correctly, in a stable and repeatable manner. These requirements are considered within the geometric domain during the design planning stage, specifically, size, suitable electric and thermal boundary conditions, number of gripping pads, and tweezing gap with respect to the size of geometric domain.
- Kinematic requirements: Maximize the tweezing (output) displacements, u_{out}, under applied input voltage, V
- Structural requirements: Maximize the structural stiffness when the ETM microgripper tweezes an object with a given stiffness. This requirement is implemented using a spring with a stiffness K. This spring can also act as a parameter for designing a stiffer or softer microgripper.

Thus, the TOM design objective is to determine the optimal topology of the geometric structure acting as a microgripper that fits within a design domain and deforms as desired when subject to electrical, thermal, and mechanical boundary conditions as shown in Figure 1. The non-linear topology optimization problem for the ETM microgripper design is defined in its discrete form as (Rubio, 2005):

$$\max_{\rho^i} \; u_{out} \qquad \text{(Output displacement)}$$

s.t.

$$\sum_{i=1}^{N} \rho^i V^i \le V^* \qquad \text{(Material constraint)} \qquad (5)$$

$$0 < \rho^i_{min} \le \rho^i \le 1 \quad for \quad i = 1...N$$

FE equations (see equations 1 up to 3)

where, V^* is the material volume constraint. A lower bound ρ^i_{min} is also specified for design variables to avoid numerical problems, as singularities of the electrical and thermal conductivity matrices, and singularities of the stiffness matrix. Here, ρ^i_{min} is chosen to be equal to 10^{-4}. Thus, numerically, regions with $\rho^i = \rho^i_{min}$ have no structural significance and they can be considered as void areas.

Figure 2 shows a flow chart of the developed optimization algorithm to solve the non-linear problem described by Eq. (5). The initial geometric domain is discretizated into finite elements, and the design variables are defined as the pseudo-density, ρ^i, with the same values in each finite element i. The optimization problem is approximated by a set of linear sub-problems by using SLP (Haftka *et al*, 1990). Thus, for each iteration, the FE problems are solved (Eqs. 1-3), the objective function is found (Eq. 5), and the respective linear optimization sub-problem is solved. In addition, for each iteration, moving limits are defined for the design variables with 5–15% of the original values, and based on continuation method, the penalization coefficients p_e, p_t are modified from 1 to 2, and p_m is changed from 1 to 3 with increments of 0.1. When each linear optimization sub-problem is solved, a new set of design variables ρ^i is obtained and the design domain is updated until convergence is reached for the defined objective function. The procedure has converged when the changes in design variables from iteration to iteration are below than 10^{-3} (Rubio, 2005). Moreover, in order to avoid the traditional mesh dependency and checkerboard (regions with alternating solid and void element) problems in topology optimization (Bendsøe and Sigmund, 2003), a filter (Cardoso and Fonseca, 1999) was implemented by using a filter radius of eight neighboring elements.

['Insert figure 2 about here']

2.3 The ETM microgripper

The overall design process of an ETM microgripper is based on topology optimization procedures shown in Figure 3. Initially, the design's geometric domain is defined and it is discretizated using 4-node quadrilateral finite elements. A general rectangular design domain is adopted for a microgripper with a pair of tweezing pads having one degree of freedom and anchored on opposite end. The microgripper was designed for operation in the normally open mode. In this mode, the holding pads will be tweezed from a certain initial gap to a desired gap only under an applied voltage to hold a micro-object. The pads will return to their initial open position due to the structural stiffness when voltage is disconnected in order to release an object. The two-pads design domain is shown in Fig. 3a using a nickel foil with a thickness of 25 μm as a workpiece with specific electrical/mechanical

boundary conditions and applied voltage. A gap between tweezing/holding pads is set to be 150 μm. Ambient temperature at the mechanical supports points is assumed. The electrical and physical properties of the nickel foil at 300 K, e.g. electrical and thermal conductivities, thermal expansion coefficient, etc., are given in Table 1. Parameters used in TOM procedure, e.g. environment temperature, volume constraint, workpiece stiffness, are presented in Table 2. The geometric domain was discretized into 4,000 isoparametric 4-node quadrilateral finite elements (see Fig. 3a). For electric and thermal analysis, each node has one degree-of-freedom (dof), a nodal voltage, and temperature, respectively. For mechanical analysis, plane stress state is assumed, where each node has two dof, horizontal (X) and vertical (Y) displacements. The TOM finds the optimum topology with an interactive process, as shown in Fig. 3b. Convergence and the optimum topology for microgripper were sketched after 95 iterations (see Fig. 3b). The TOM solution is also simulated and validated using a commercial FE program ANSYS/multiphysics™. The simulation results are shown in Figure 4 (Note: more details about simulations are in Section 3). Finally, the design-development cycle is finished when the optimum ETM microgripper is manufactured and performance evaluated (see Figure 5 and Section 4).

['Insert table 1 about here']

['Insert table 2 about here']

['Insert figure 3 about here']

The designed microgripper (see Fig. 3b) has a symmetric monolithic structure consisting of the actuation mechanism (microactuator) and the gripping mechanism together. This differs from the traditional approach of using a tweezing mechanism attached to a microactuator while both act as separate but interconnected kinematic entities. The monolithic symmetric structure delivered by TOM provides several performance advantages, such as, a symmetrical distribution of the material, voltage, temperature and displacements along the entire microgripper body, which does not require post-fabrication assembly. In the proposed design, the microactuator is a combination of several actuation beams, which collectively magnify the output in-plane displacements of the gripping mechanism consisted of two symmetrical arms and pads. The driving voltage is applied to two fixed electric pads at the bottom. In other words, the designed microgripper provides two combined functionalities, e.g., simultaneous actuation and tweezing actions, by one structural body which cannot be separated into two independent kinematic micro-mechanisms (see Fig. 4). Combining the actuation and gripping mechanisms into one monolithic structure significantly reduces design complexity and increases structural stiffness, e.g. avoiding flexural hinges, without sacrificing the performance.

3 Finite Element simulations

The numerical evaluation of the ETM microgripper is performed by using the coupled electro-thermo-mechanical analysis capability of the ANSYS/Multiphysics™ software, and by building a CAD model

of the optimum topology available from the TOM procedure. A complete simulation of ETM microgripper behavior consists of three independent finite element calculation steps. Initially, the voltage distribution is calculated through an electrical analysis. Then, the induced heat is calculated through a thermal analysis, and, finally, the program transfers the temperature data to the mechanical solver as all steps are shown in Figure 4. The dimensions and material properties of the 3D FE model are identical to the microgripper prototype and it is meshed using a SOLID 98 type element. The simulation steps (see Fig. 5) are based on microgripper simulation procedure described in Section 5.4. This procedure considers convective heat transfer, thermal boundary conditions at the fixed anchors, and temperature dependent material properties, in order to compare the acquired numerical results with data from the experimental performance evaluation.

['Insert figure 4 about here']

Figure 4a shows the topology optimized design of the microgripper used for simulation and fabrication. The voltage, temperature, and von Mises stress distributions were calculated for the optimum topology when the microgripper was driven by an input voltage of 4.50 V and results are shown in Figures 4b, 4c and 4d, respectively. When the input voltage is turned on, the electric current runs through the conductive metallic structure of the microgripper causing thermal expansion (Joule heating) of all individual actuation beams, and consequently, the entire monolithic structure expands in such a way that the gripping pads move towards each other producing output in-plane tweezing displacements and force (see Fig. 4d where all displacements are increased for better visualization of the tweezing motion). It was noticed during simulation that there were two regions of the microgripper's structure that functioned differently, see Fig. 4b and 4c. There is an "active region" represented by an actuator and a "passive region" represented by a gripping mechanism. The "active region" has high temperatures, stresses (specifically, close to fixed anchors), and electric current density. In this region, all actuation beams expands mostly linearly and act as kinematic prismatic or sliding joints. The combination of these linear expansions generates complex movements of the entire structure causing left and right sides to move forward and rotate inward (see Fig. 4d). On the contrary, the "passive region" has relatively negligible current density, temperature and von Mises stresses. The "passive region" is a more compliant area where structural beams have a larger rotational movement initiated by the "active region" and act as kinematic revolute joints. The presence of these two regions allows avoiding impact of high actuation temperatures, electric current and mechanical stresses while tweezing/holding an object.

4 Microfabrication of microgripper prototype

A laser micromachining system developed at NRC-IMTI was used for microfabrication of the microgripper prototypes. The system was equipped with a Q-switched diode pumped solid state Nd: YAG laser operating at a wavelength of 355 nm with pulse-to-pulse energy stability of less than 5% rms up to 30 kHz for linear polarization in the TEM_{00} mode. The laser beam was focused on to the workpiece surface by a combination of beam expander and a focusing objective. The three-axis CNC-based motion system consisted of precision translation stages with linear motors for X and Y

movements with a positioning accuracy of 0.5 μm. Z-axis translation stage with ball-screw drive having a positional accuracy of 1 μm was mounted vertically. Both the laser and the motion system were controlled and synchronized in time and space using in-house developed software, which enabled the setting up of the process parameters as well as the desired toolpath trajectory with minimal dynamic errors. The parameters of the laser-material removal process, such as laser power, pulse repetition rate, working distance, and feed rate, were optimized in order to achieve accuracy and precision of the fabricated prototype within +/– 1 μm.

['Insert figure 5 about here']

['Insert figure 6 about here']

['Insert table 3 about here']

Figure 5 shows an ETM microgripper prototype fabricated from a pure nickel foil with a thickness of 25 μm having overall dimensions of 2478 (W) μm x 1000 (L) μm and a smallest width of the structural beams of 17 μm. The machining quality of the fabricated microgripper was analyzed through optical measurements and using a scanning electron microscope. An *Olympus* optical stereo microscope (model SZX12) and *VisionGauge*™ software were used to measure the geometry of fabricated prototypes with an accuracy of 0.1 μm. Figure 6 shows the geometric quality of the machined actuation beams, gripping arms, and tweezing pads, the most critical design element related to the performance of the microgripper. As it was expected (Bordatchev *et al*, 2005) due to nanosecond pulse duration of the laser pulses, the actuation beams had rough side-walls and significant amount of burrs and build-ups as a result of the laser-material interactions. During the laser material removal, burrs and build-ups in the sharp corners of the internal geometric elements were often re-adhered to the machined surface fusing the internal element to the rest of the structure. Table 3 summarizes the dimensional accuracy in terms of desired/actual dimensions and absolute accuracy. Note that some dimensions of the fabricated prototypes were machined within sub-micron accuracy, for example, the gap between gripping pads and the thickness of the thinnest structural beam represents feature accuracy of 0.2 μm and 0.5 μm respectively. This superior accuracy was achieved mainly due to high positional accuracy of the motion system, proper synchronization of motions, laser on/off events and the desired tool path trajectory.

5 Characterization

5.1 Experimental Set-up and Procedure

The experimental setup for evaluating the static and dynamic performance characteristics of the fabricated microgripper is shown in Figure 7. The setup consists of an *Agilent* power supply (model A3631A), 1 Ohm power resistor, *LeCroy* digital oscilloscope "*WaveRunner*" (model LT354), *Olympus* optical microscope (model SZX12) with a Basel CMOS camera (model A602f) under *VisualGauge*™ software control, and desktop computer. The microgripper was mounted on a specially designed and

fabricated substrate made of a small piece of 1 mm PCB and it was wired to a standard electrical connector. Two channels of the oscilloscope were connected to the circuit: one to measure the applied voltage across the microgripper, and the other to measure the applied current across the power resistor. The total resistance of the connecting wires was 1.4 Ohm.

['Insert figure 7 about here']

The performance evaluation involved the following steps. By switching on the power supply, voltage and current were applied to the microgripper as a step input. Simultaneously, applied voltage and current were recorded by the digital oscilloscope, and the planar tweezing displacements for a single gripper pad were captured by a CMOS camera through the optical microscope for further analysis. As a result, two step response characteristics with respect to the applied current were obtained – electrical (current vs voltage) and mechanical (current vs displacement). Each performance test took 3 seconds which was sufficient to achieve steady state. Electrical step responses were recorded by the oscilloscope; while mechanical step response was obtained through analysis of the captured images using National Instrument™ Automation Inspection software. Note that during experiments all applied currents were kept below 2.6 A, which is a functional limit for a designed microgripper before buckling and overheating effects occur.

To achieve smooth tweezing displacements for the microgripper, all testing experiments were performed under constant current control (CCC) scheme where the desired current was set by a power supply and the voltage across microgripper was generated in accordance to the actual electric resistance and mechanical performance of the microgripper. The CCC scheme prevents current spikes, burning of the microgripper, and displacement overshoot. Figure 8 shows the typical electrical step response characteristics, such as, applied current, $I(t)$, and produced voltage, $V(t)$, and mechanical step response characteristic, tweezing displacement, $x(t)$, obtained under an applied current of 2.0 A.

['Insert figure 8 about here']

The performance of the fabricated microgripper was obtained experimentally as dynamic responses of the produced voltage and tweezing displacements with respect to the applied constant current with a range of {0.2, 0.4, ..., 2.6} A. Based on the experimental performance, the following electro-mechanical static and dynamic characteristics were determined and studied:

- the static tweezing displacement with respect to applied power (see Fig. 9),
- the calculated overall resistance with respect to applied power (see Fig. 9), and
- the dynamic tweezing displacement with respect to applied current (see Fig. 10).

5.2 Static Performance Characterization

Figure 9 shows the static electro-mechanical performance characteristics as functions of maximum tweezing displacements at steady state and actual resistance with respect to applied electric power.

The tweezing displacements increase linearly along with a corresponding increase in applied power. It is necessary to note that the microgripper produces two motions in X and Y directions simultaneously because of even heating distribution of the material. It means that the designed structure has two functionalities performing linear (along Y axis) and tweezing (along X axis) actions simultaneously. However, the designed structure re-directs thermal deformation producing the required tweezing displacements. For example, under the maximum applied power of 2.32 W, the microgripper generated tweezing displacement of 25.5 μm and 33.2 μm along X and Y axes, respectively. The slope of displacement-power function represents both the effectiveness and efficiency of a microgripper to generate linear and tweezing displacements with respect to the consumed power, e.g., 10.5 μm/W and 14.1 μm/W for X and Y axes, respectively. Therefore, the design acts more as an actuator than as a gripper and this actual performance should be taken into consideration for further design optimization and proper practical applications.

['Insert figure 9 about here']

Another significant drawback of the designed microgripper is its electrical resistance (see Fig. 9), which is significantly less than the resistance of connection wires. It is well known fact that when electric current passes through the monolithic metal structure, the structure will be heated up by Joule heating and it will be thermally expanded with a certain thermal expansion coefficient. However, the heating causes an increase in material resistance and changes the thermal expansion coefficient. Because different design elements of the microgripper structure have different temperatures (see Fig. 4c), each element will have a specific thermal expansion coefficient and electric resistance. This fact creates significant challenges in modelling and simulation of microgripper performance with respect to the actual performance. This increment in resistance is a significant factor for power consumption and therefore overall performance. Actual resistance of ETM microgripper during functioning was calculated using measured applied current and voltage, and Fig. 9 shows significant increase in resistance of the microgripper with respect to the applied power. For instance, the microgripper increased its resistance value from 0.068 Ohm to 0.336 Ohm when the power increased from 0.003 W to 2.32 W non-linearly, which could be attributed to the complex temperature distribution along the structure.

5.3 Dynamic Performance Characterization

The dynamic electro-mechanical performance of the fabricated microgripper prototype was studied based on the analysis of the transient state of the step response function with respect to applied current, generated voltage, and tweezing/actuating displacements. Figure 10 shows the dynamic mechanical performance of the microgripper with respect to an applied current within a range of {1.2, 1.4, ..., 2.6} A in terms of tweezing (along X axis) and actuating (along Y axis) displacements. All response characteristics are not periodic; they are without oscillations and overshoots that is similar to the standard behaviour of electro-thermo-mechanically driven microsystems (Bordatchev and Nikumb, 2005, Lai *et al*, 2006, Zeman *et al*, 2006). Dynamic electrical performance characteristics for the same range of applied current is similar to typical characteristics shown in Fig. 8. It is also necessary

to note (see Fig. 8) that the applied current of 2.0 A reaches its steady state almost instantly with a transient response time of 6 ms. Simultaneously, the voltage rises to a steady state of 3.32 V across the microgripper during same response time. It is general performance for electro-thermo-mechanically driven micro-mechanisms (Lai *et al*, 2006, Zeman *et al*, 2006) that the mechanical response has significantly longer transient state, because of the physics of thermo-mechanical processes, where considerable time is required to obtain a balance between Joule heating and natural convection processes within the microgripper solid body structure. A duration of the transient state of electrical responses is very short, e.g. 6 msec (see Fig. 8) *vs* 3 sec for mechanical response.

['Insert figure 10 about here']

5.4 Matching Finite Element model and Experimental Results

Preliminary results of microgripper simulation were shown in Section 3. However, these results do not adequately describe the microgripper's dynamic performance. Therefore, there is a need for a simulation procedure in order to understand modelling inaccuracies and to find an FE model which will accurately match the numerical results with the experimental measurements. Thus, preliminary considerations are necessary to simulate the ETM microgripper, such as, sensitivity studies of mesh size, boundary conditions and material properties. First, it was necessary to determine how the mesh size affects the results, thus, a convergence study was conducted on meshing by using 4,500 to 31,000 finite element mesh-sizes keeping some parameters constant, e.g., a thermal convection coefficient of 150 $W/m^2 \cdot K$, and an input voltage of 1.25 V. A mesh size larger than 19,000 finite elements showed convergence with low computation cost. The convergence was studied by analyzing the X and Y displacement of the top corner of the left gripping pad, and the maximum electrical current and temperature were obtained from an entire microgripper structure.

Likewise, the correct application of electrical and thermal boundary conditions is important, due to the fact that they can affect the final result considerably. The voltage was applied to the central node of the mechanical anchor (electrical pad). Two studies were developed considering the influence of thermal boundary conditions (Mankame and Ananthasuresh, 2001) (see Fig. 4): (i) imposing the ambient temperature at the bottom of the mechanical anchors (called essential thermal boundary condition or ETBC), and (ii) imposing ambient temperature at the side areas to each anchor. Other thermal boundary conditions are possible, e.g., by imposing the ambient temperature at the substrate (called natural thermal boundary condition or NTBC). This condition leads to more accurate results for displacement and current; however, it causes a higher solution time, since the substrate must also be simulated. The difference between first and second thermal boundary conditions was very small. Nevertheless, the ETBC condition was chosen in view of reducing the solution time and producing numerical values close to the experimental performance. By measuring the open-close tweezer displacement with a driven voltage of 1.25 V and a thermal convection coefficient of 150 $W/m^2 \cdot K$, the ETBC condition is within 20% of the actual displacements.

On the other hand, to reduce the difference among FE and experimental results, it was important to determine the approximate natural thermal convection coefficient value used in experimental tests. Consequently, by keeping some parameters constant (300 K on the anchor

temperature, 1.25 V for driven voltage, discretization of 19,476 finite elements, and ETBC condition), the influence of change of thermal convection coefficient on the microgripper behavior could be studied. Displacements of one arm tip were obtained for a range of thermal convection coefficient values of {0, 50, 100, 150, 200, 500, 1000, 3000,..., 3600} $W/m^2 \cdot K$, and all areas on the model were assumed to contribute to heat exchange with environment. The thermal convection coefficient values between 100 up to 200 $W/m^2 \cdot K$ generate the better results minimizing the FE-experimental error. However, this coefficient is a constant "threshold", because, its experimental determination can be particularly troublesome, and, sometimes, no consensus can be obtained between theoretical and experimental values. A thermal convection coefficient value equal to 150 $W/m^2 \cdot K$ was chosen once it produces the closest output displacement to experimental results.

Finally, to complete the FE model of the microgripper, the microgripper behavior was simulated considering non-dependent-temperature material properties (the relation property versus temperature is constant during all the simulation time) and dependent-temperature material properties. In the last case, electrical conductivity was constant and no convergence was reached. Than temperature-dependent electrical conductivity and higher input voltage (more than 1.25 V) were applied. In this case, very large displacements and temperatures were obtained (according to simulation temperatures between 700 – 1400 °C approximately). Both property simulations assume non-linear output displacement. The environmental temperature adopted was 300 K and the convection coefficient value equal to 150 $W/m^2 \cdot K$. Figure 11 shows the comparison of tweezing displacements (along X axis) simulated results obtained considering temperature-dependent and independent material properties with respective experimental data for input voltage values of {0.30, 0.61, 0.93, 1.25, 1.59, 1.93, 2.24, 2.59, 2.94, 3.31, 3.71, 4.16, 4.56} V.

['Insert figure 11 about here']

In addition, it can be observed in Fig. 11 that better results were obtained by considering dependent-temperature material properties in relation to non-dependent-temperature curve. Thus, for an input voltage between 1 V and 3.5 V, the percentage difference between experimental and simulated data, in both models, ranges from 8.5 % to 46 %. However, when the input voltage is more than 3.3 V the percentage difference for non-dependent-temperature material curve continually raises from 8.5 % to 38 %. This percentage difference for dependent-temperature material curve is continually diminishing from 41 % to 4.5 %. These differences between experimental and numerical results can be produced for non-temperature-dependent electrical conductivity. Moreover, for non-dependent-temperature model, the difference increases for higher voltages, and, consequently, higher operating temperatures (above 600 K), because no variation of the material properties with temperature was assumed. On the contrary, for higher voltages, the temperature-dependent model generates small differences, as shown in Fig. 11. In addition, these differences arise due to no radiative heat loss assumption, which becomes significant in high temperatures. This is especially true for microgrippers and microdevices as a whole, where the ratio of surface area to volume increases with miniaturization. Moreover, mismatch can cause due to inadequate thermal convection coefficient and temperature-dependent material properties used for simulation.

6 Summary and conclusions

This paper presents a systematic study o f the topology optimized design, microfabrication, and static/dynamic performance characterization of an electro-thermo-mechanical microgripper. The microgripper was designed using a continuum topology optimization algorithm based on a spatial filtering technique and considering different penalization coefficients for different material properties during the optimization cycle. The microgripper design consisted of a symmetric monolithic metallic 2-D structure as a complex combination of rigid links integrating both the actuation and gripping mechanisms. The numerical simulation was performed studying the effect of the convective heat transfer, thermal boundary conditions at the fixed anchors, and microgripper performance with and without considering temperature-dependent material properties. The microgripper was fabricated from a 25 μm thick nickel foil using the laser microfabrication technology, and its performance was experimentally evaluated using a constant current control scheme. The static and dynamic electro-mechanical characteristics were analyzed as step response functions with respect to tweezing/actuating displacements, applied current/power, and actual electric resistance. For a microgripper prototype with overall dimensions of 1 mm x 2.5 mm, the maximum tweezing and actuating displacements of 25.5 μm and 33.2 μm along X and Y axes, respectively, were obtained under an applied power of 2.32 W. Experimental performance was compared with finite element modeling simulation results.

The following conclusions can be drawn from these studies:

1. The microgripper, being a complex electro-thermo-mechanically driven dynamic microsystem, is capable of generating predictable, smooth and accurate tweezing and positioning motions under the constant current control operation without an overshoot or destructive current/voltage spikes.
2. The topology optimization methodology can be successfully applied as systematic tool to design such type of compliant micro-mechanisms and electro-thermally actuated microgrippers.
3. The finite element modelling based numerical simulation using the temperature-dependent material properties gave the best validation of experimentally obtained data, e.g. for an input voltage of 4.56 V, the simulated tweezing displacements are within 4.5 % difference.
4. The microgripper can be used as a miniature end-effector for handling and manipulation of miniature components and objects in a variety of applications including mechanical micro-assembly, micro-robotics and biological cell manipulation.
5. For future work, an electrical current constraint on optimization problem can be implemented, in order to design a microgripper that operates with less driving voltage and, therefore, less operating temperature reducing actual plastic deformation of the entire structure and increasing performance durability and repeatability.

Acknowledgments

This paper is the result of a collaboration between Escola Politécnica da Universidade de São Paulo, São Paulo, Brazil and NRC-IMTI, London Ontario, Canada. This study was supported by FAPESP – São Paulo State Foundation Research Agency, through the doctoral fellowship Nº. 05/01762-5, and NSERC-Canada Discovery Grant R3440A01. The authors thank Mr. Mahmud-Ul Islam, Director,

Production Technology Research, NRC-IMTI, and Dr. Suwas Nikumb, Group Leader, Precision Fabrication Processes, NRC-IMTI, for their continued support in this work.

References

Ananthasuresh G K 2003 Optimal Synthesis Methods for MEMS, Boston: Kluwer Academic Publishers

Belfiore P and Pennestri E 1997 An Atlas of linkage-type robotic grippers, Mechanics and Machine Theory 32: 811-833

Bendsøe M P and Sigmund O 2003 Topology Optimization: theory, Methods and applications. Springer, Berlin: 71 – 152

Bendsøe M P and Sigmund O 1999 Material Interpolations Schemes in Topology Optimization, Archive of Applied Mechanics 69: 635-654

Bordatchev E V and Nikumb S K 2005 Electro-thermally driven microgrippers for micro-electro-mechanical systems applications, J. Microlith., Microfab., Microsyst., **4**(2): 23011-1-7

Bordatchev E V, Lai Y and Nikumb S K 2005 Comparative Analysis of Microactuators Fabricated by the Femtosecond and Nanosecond Laser Micromachining, Proceedings of 5th Intl. Conf. of Laser Ablation, September 11-16, 2005, Banff, Alberta, Canada, 2005, paper ThPO55.306: 377

Bordatchev E V, Nikumb S K and Hsu W 2004 Laser micromachining of the miniature functional mechanisms, Proceeding of SPIE, 5578: 579-588

Cardoso E L and Fonseca J S O 1999 Intermediate density reduction and Complexity Control in the Topology Optimization, Proceeding of XX CILAMCE, Brazil, ???

Choi H S, Lee D C, Kim S S and Han C S 2005 The development of a microgripper with a perturbation-based configuration design method, Journal of Micromechanics and Microengineering, **15**(6): 1327-1333

Goldfarb M and Celanovic N 1999 A flexure-based gripper for small-scale manipulation, Robotica, **17**(2): 181–188

Guckel H, Klein J, Christenson T, Skrobis K, Laudon M and Lovell E G 1992 Thermo-magnetic metal flexure actuators, In: IEEE Solid-State Sensors and Actuators Workshop: 73–5

Haftka R T, Gürdal Z and Kamat M P 1990 Element of Structural Optimization, Dordrecht; Boston: Kluwer Academic Publishers

Howell L L 2001 Compliant Mechanisms, New York: Wiley

Jonsmann J 1999 Technology Development for Topology Optimized Thermal Microactuators, Ph.D. Thesis, Technical University of Denmark, Mikroelektronik Centret, Denmark: 8 – 28

Kim D H, Kim B and Kang H 2004 Development of a piezoelectric polymer-based sensorized microgripper for microassembly and micromanipulation, Microsystem Technologies-Micro-and Nanosystems-Information Storage and Processing Systems, **10**(4): 275-280

Kohl M, Just E, Pfleging W and Miyazaki S 2000 SMA microgripper with integrated antagonism Sensors Actuators A 83: 208–13

Kohl M, Krevet B and Just E 2002 SMA microgripper system Sensors Actuators A 97–98: 646–52

Lai Y, Bordatchev E V, Nikumb S K and Hsu W 2006 Performance Characterization of In-plane

Electro-thermally Driven Linear Microactuators, Journal of Intelligent Material Systems and Structures, **17**(10): 919-929

Lambert P, Seigneur F, Koelemeijer S and Jacot J 2006 A case study of surface tension gripping: the watch bearing, Journal of Micromechanics and Microengineering, **16**(7): 1267-1276

Lee S, Lee K and Lee S 2002 Fabrication of an electrothermally actuated electrostatic microgripper. International Journal of Nonlinear Science and Numeric Simulations, 3: 789–93

Mankame N D and Ananthasuresh G K 2001 Comprehensive thermal modeling and characterization of an electro-thermal-compliant microactuator, Journal of Micromechanics and Microengineering, 11: 452-462

Menciassi A, Eisinberg A, Mazzoni M and Dario P 2002 A sensorized μelectro discharge machined superelastic alloy microgripper for micromanipulation: simulation and characterization, Proc. 2002 IEEE/RSJ Int. Conf. of Intelligent Robots and Systems, Lausanne, Switzerland: 1591–5

Menciassi A, Eisinberg A, Izzo I and Dario P 2004 From "macro" to "micro" manipulation: models and experiments, IEEE-ASME Transactions on Mechatronics, **9**(2): 311-320

Millet O, Bernardoni P, Regnier S, Bidaut P, Tsitsiris E, Collard D and Buchaillot L 2004 Electrostatic actuated micro gripper using an amplification mechanism, Sensors and Actuators A-Physical, 114: 371-378

Moulton T and Ananthasuresh G K 2001 Micromechanical devices with embedded electro-thermal-compliant actuation, Sensors and Actuators A, 90: 38-48

Nguyen N T, Ho S S, and Low C L-N 2004 A polymeric microgripper with integrated thermal actuators, Journal of Micromechanics and Microengineering, 14(7): 969-974

Park J and Moon W 2005 The systematic design and fabrication of a three-chopstick microgripper, International Journal of Advanced Manufacturing Technology, **26**(3): 251-261

Park J and Moon W 2003 A hybrid-type micro-gripper with an integrated force sensor, Microsystem Technologies – Micro- and Nanosystems-Information Storage and Processing Systems, **9**(8): 511-519

Perez R, Agnus J, Clevy C, Hubert A and Chaillet N 2005 Modeling, fabrication, and validation of a high-performance 2-DoF piezoactuator for micromanipulation, IEEE-ASME Transactions on Mechatronics, 10(2): 161-171

Roch I, Bidaud P, Collard D and Buchaillot L 2003 Fabrication and characterization of an SU-8 gripper actuated by a shape memory alloy thin film, Journal of Micromechanics and Microengineering, 13(2): 330-336

Rubio W M 2005 Electrothermomechanical MEMS design base on Topology Optimization Method, Master Thesis, Escola Politécnica da Universidade de São Paulo

Sanchez-Salmeron J, Lopez-Tarazon R, Guzman-Diana R and Ricolfe-Viala C 2005 Recent development in micro-handling systems for micro-manufacturing, Journal of Materials Processing Technology, 167: 499-507

Sigmund O 2001 Design of Multiphysics Actuators Using Topology Optimization – Part I: One-Material Structures, Computer Methods in Applied Mechanics and Engineering, Denmark: 6577–6604

Tsai Y C, Lei S, and Sudin H 2005 Design and analysis of planar compliant microgripper based on kinematic approach, Journal of Micromechanics and Microengineering, 15(1): 143-156

Volland B E, Heerlein H and Rangelow I W 2002 Electrostatically driven microgripper, Microelectron.

Eng., 61–62: 1015–23

Wierzbicki R, Houston K, Heerlein H, Barth W, Debski T, Eisinberg A, Menciassi A, Carrozza M C and Dario P 2006 Design and fabrication of an electrostatically driven microgripper for blood vessel manipulation, Microelectronic Engineering, 83: 1651-1654

Zeman M, Bordatchev E and Knopf G 2006 Design, kinematic modeling and performance testing of an electro-thermally driven microgripper for micromanipulation applications, Journal of Micromechanics and Microengineering, 16(8): 1540-1549

Zesch W, Brunner M and Weber A 1997 Vacuum tool for handling micro-objects with a nanorobot, IEEE International Conference on Robotics and Automation, 2: 1761-1766

LIST OF TABLES

Table 1. Electrical and physical properties of the nickel foil at 300 K

Electrical conductivity (1/Ohm·m)	6.5×10^{6}
Thermal conductivity (W/m K)	92.4
Thermal expansion coefficient (K^{-1})	13×10^{-6}
Young's modulus (Pa)	2.064×10^{11}
Poisson's ratio	0.31

Table 2. Parameters used in TOM procedure

Environment temperature (K)	300
Volume constraint	30%
Workpiece stiffness, K (N m)	10000
Initial guess for pseudo-densities	0.5
Initial penalization coefficients	1
Final electrical penalization coefficient, p_e	2
Final thermal penalization coefficient, p_t	2
Final mechanical penalization coefficient, p_m	3

Table 3. Geometry evaluation

	desired dimension, μm	actual dimension, μm	absolute accuracy, μm
smallest structural beam	17.0	17.5	0.5
actuation beam	25.0	25.8	0.8
actuation beam	38.0	37.4	0.6
actuation beam	40.0	40.8	0.8
gap between gripping pads	150.0	149.8	0.2
overall width	1000.0	1000.9	0.9

LIST OF FIGURES

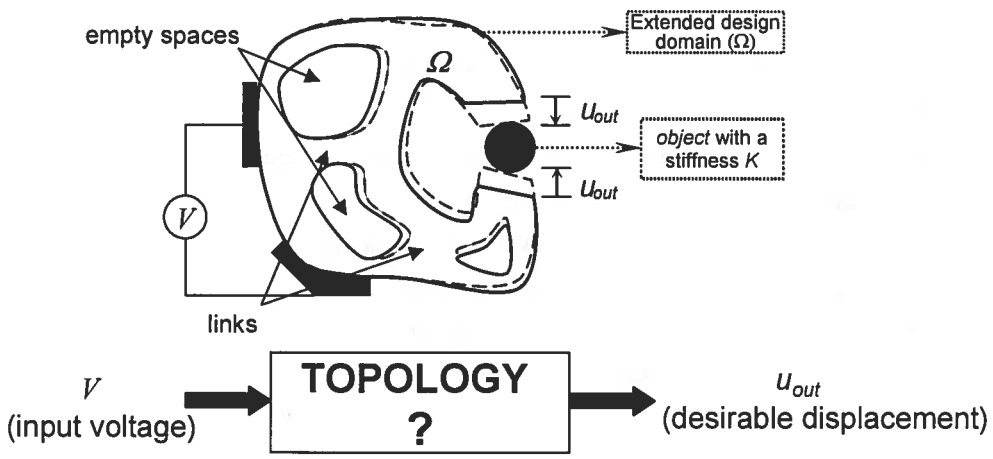

Figure 1. Concept of the topology optimization problem with respect to an ETM microgripper's design.

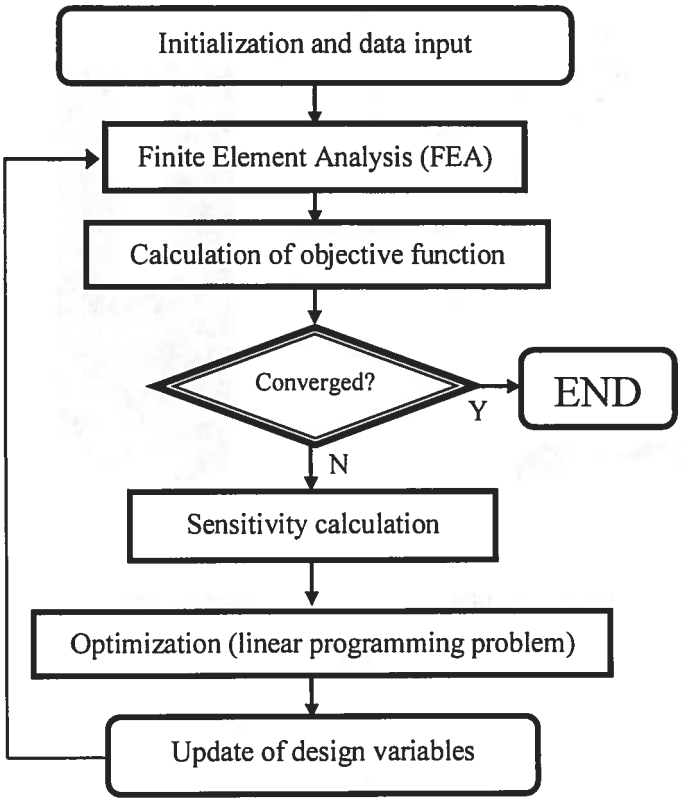

Figure 2. Flow chart of the topology optimization algorithm.

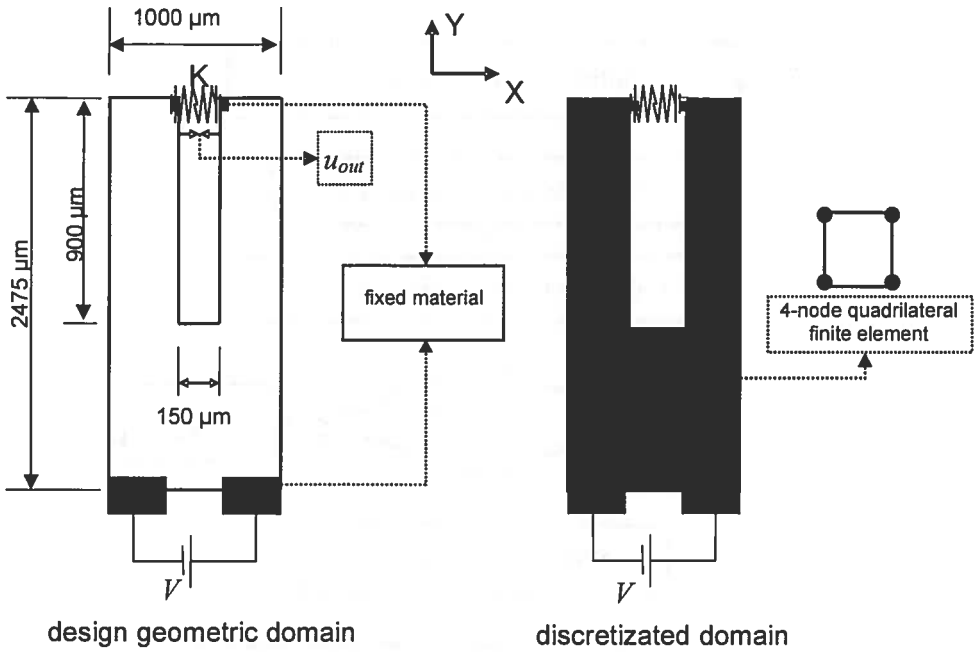

(a)

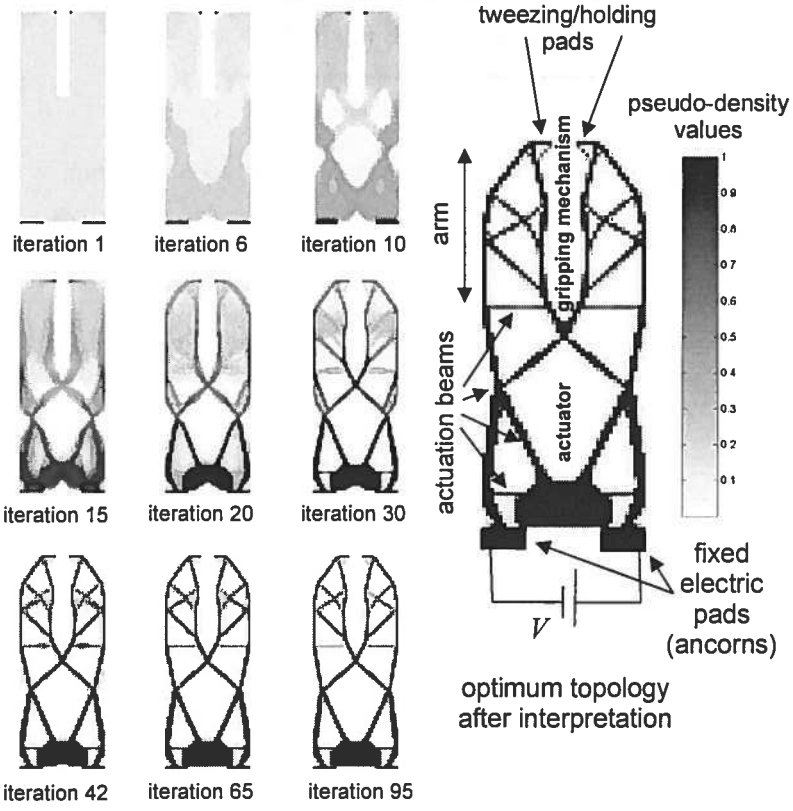

(b)

Figure 3. Overall design process of an ETM microgripper based on topology optimization; (a) extended design geometric domain (dimensions in µm) and design domain after discretization by finite elements; (b) TOM iterative process with the optimum topology.

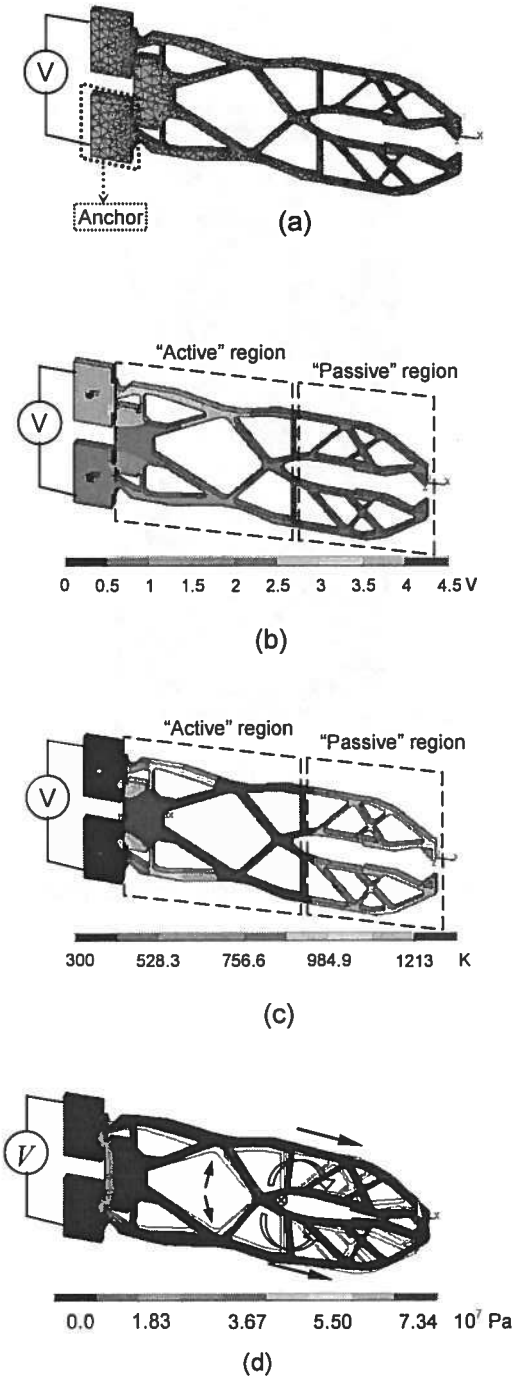

Figure 4. Complete FE simulation of the ETM microgripper: (a) mesh of the topology optimized design; (b) voltage distribution; (c) temperature distribution; (d) von Mises stress distribution of the deformed geometry.

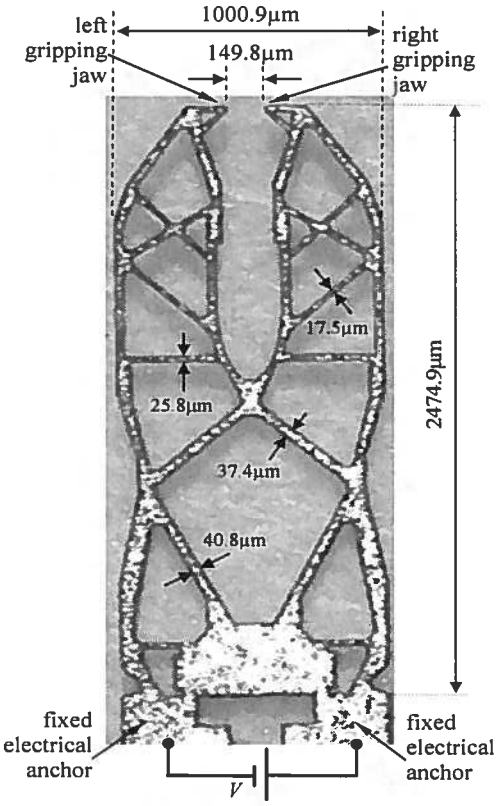

Figure 5. Fabricated ETM microgripper prototype.

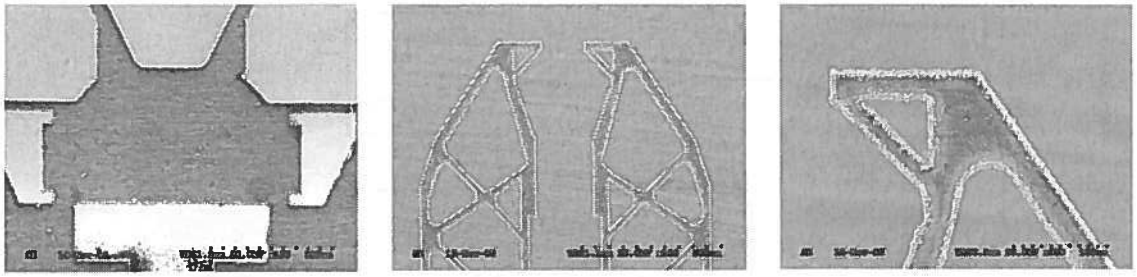

a) actuation beams b) tweezing arms c) gripping pads

Figure 6. Geometric quality of the actuation beams, tweezing arms, and gripping pads.

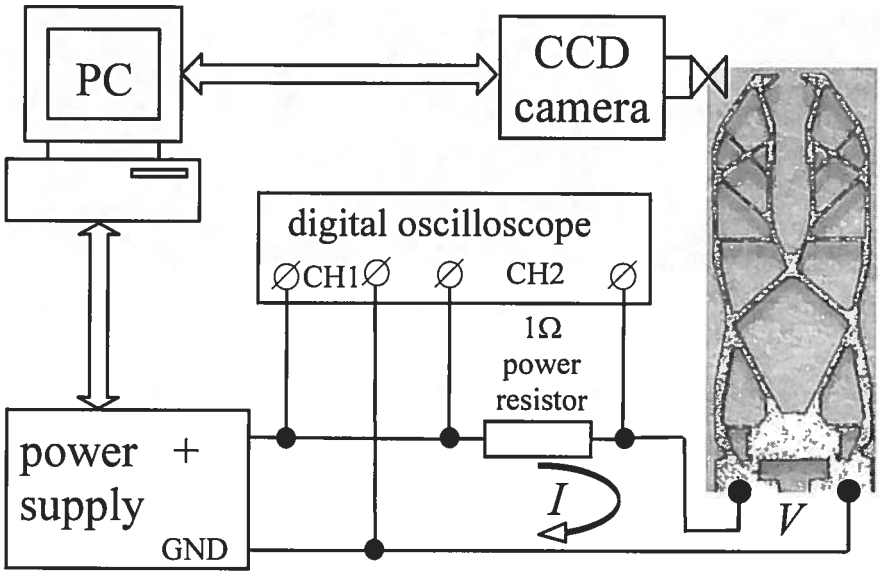

Figure 7. Experimental setup for testing microgripper performance.

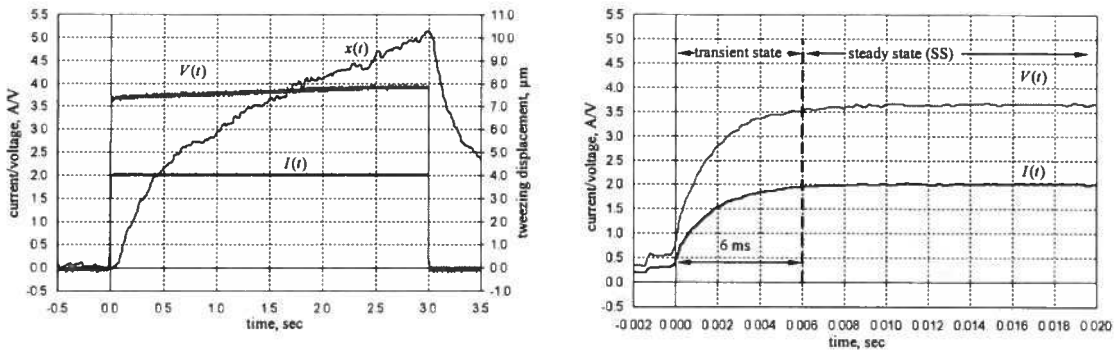

Figure 8. Typical electrical and mechanical characteristics of microgripper performance (under an applied current of 2.0A).

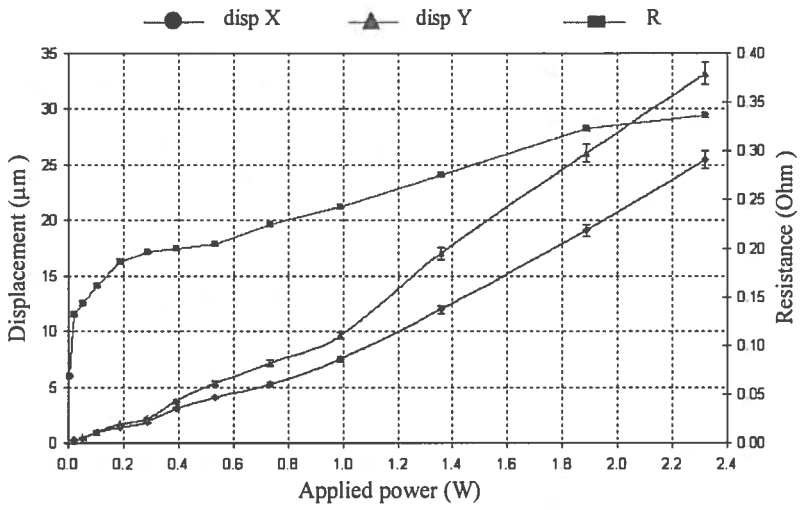

Figure 9. Static electro-mechanical performance characteristics.

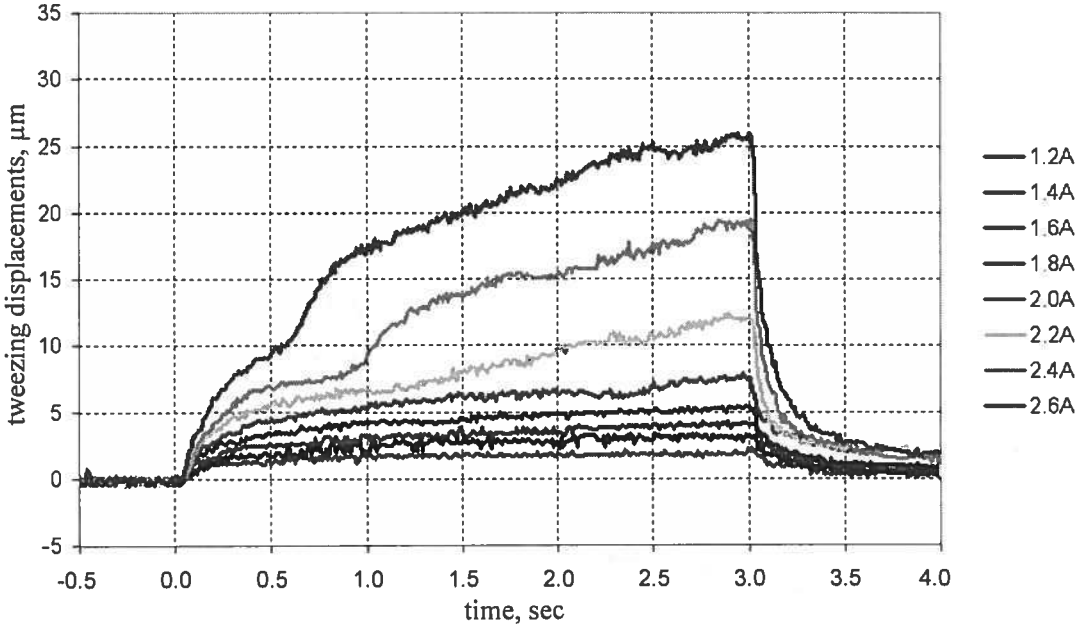

a) tweezing displacements (along X axis)

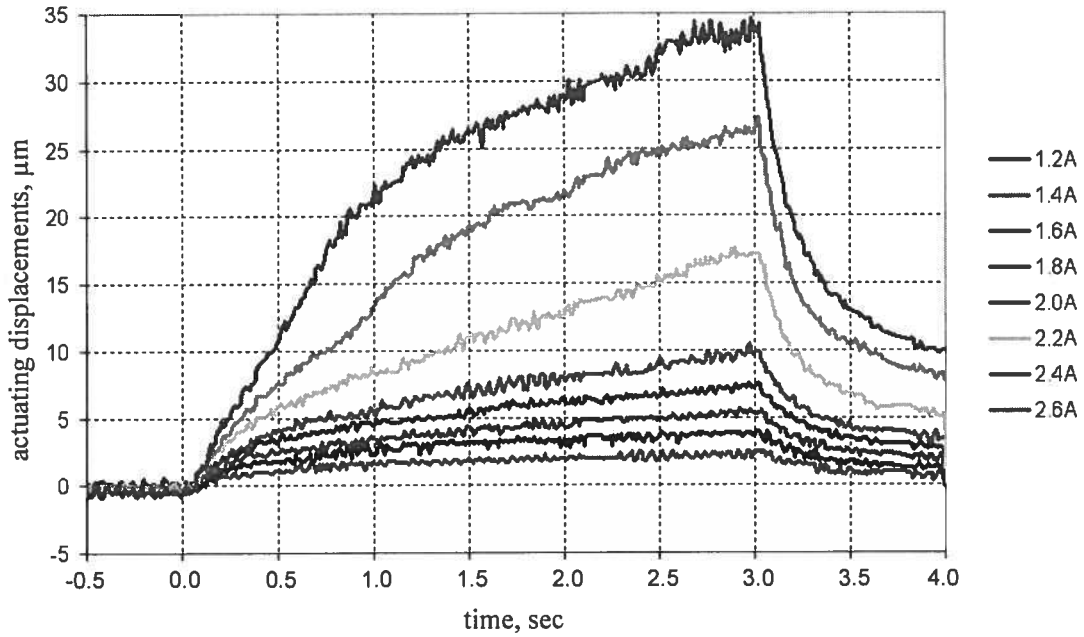

b) actuating displacements (along Y axis)

Figure 10. Dynamic mechanical performance characteristics (left pad).

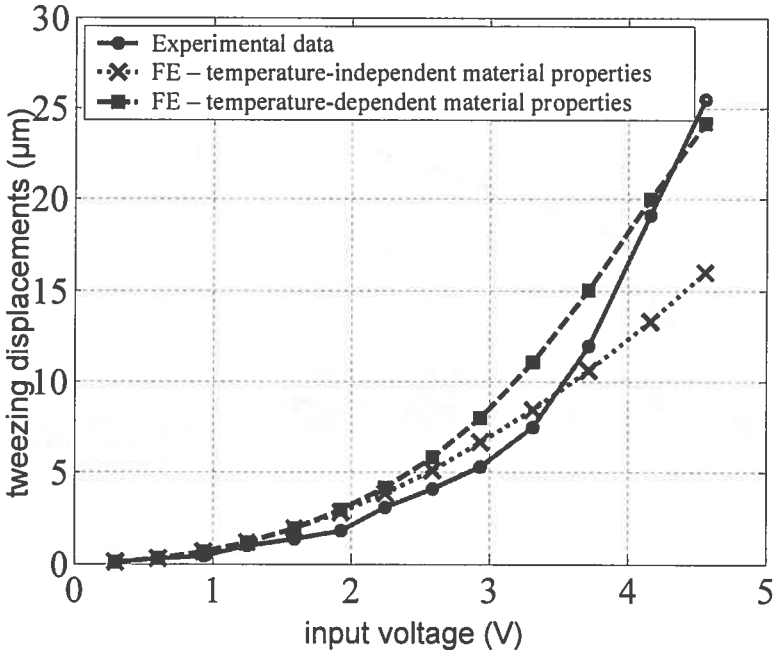

Figure 11. Comparison of simulated and experimentally obtained tweezing displacements.